Caving 2022 - Y Potvin (ed.)

doi:10.36487/ACG_repo/2205_65

Application of rock mass strength scale effect at Cadia East mine

MA Fuenzalida *Itasca Consulting Group, Inc., USA*

C Orrego *Newcrest Mining Limited, Australia*

E Ghazvinian *Itasca Consulting Group, Inc., USA*

ME Pierce *Pierce Engineering, USA*

Abstract

The relevance of the scale effect when considering rock mass strength in different aspects of mine design in a caving mine is critical. A proper understanding of rock mass strength at different scales is required to appropriately forecast cave growth, subsidence, infrastructure and footprint stability.

Evidence of rock mass strength scale effect is studied at Cadia East mine by performing a back-analysis of 1) the large-scale subsidence, and 2) stability performance of a crusher chamber.

A methodology to account for the scale effect is proposed by fitting a power-law function to the results of the back-analysis. The fitted equation is then verified based on an improved rock mass knowledge derived from a recent systematic point load test campaign.

The proposed approach serves as a framework to incorporate the scale effect in the rock mass strength in the design for future panels at Cadia East mine.

Keywords: *scale effect, rock mass strength, subsidence, stability, crusher chamber*

1 Introduction

Cadia East mine is located in Central New South Wales, Australia, and consists of three active panels PC1, PC2 and PC2-3 (Figure 1). PC1 and PC2 (conformed of PC2-1 and PC2-2) extraction levels are located approximately 1,200 m and 1,400 m below ground surface respectively making it one of the deepest active caving mines in the world.

A proper understanding of rock mass strength at different scales is required to appropriately forecast cave growth, subsidence, infrastructure and footprint stability. For example, if the rock mass strength at the tunnel scale is overestimated this can have significant implications in terms of the long-term stability and overall production capacity of the cave mine. Conversely, if the rock mass strength at the cave scale is underestimated it would affect caveability forecasting, resulting in a lower caving rate in which would directly affect the production rate and associated potential risks of subsidence zone growth and air gap formation.

Evidence of rock mass strength scale effect is studied at Cadia East mine by performing a back-analysis at two different scales: 1) the large-scale caving-induced subsidence and 2) the stability performance of a crusher chamber at PC2-1.

This paper begins with a description of the empirical evidence on the scale effect of rock strength. This is followed by the back-analysis conducted at Cadia in 2020 to derive the rock mass strength that would match the observed behaviour at the cave and tunnel scale. A power-law fit is applied based on the results of the back-analysis providing an overall understanding of rock mass strength at varying scales.

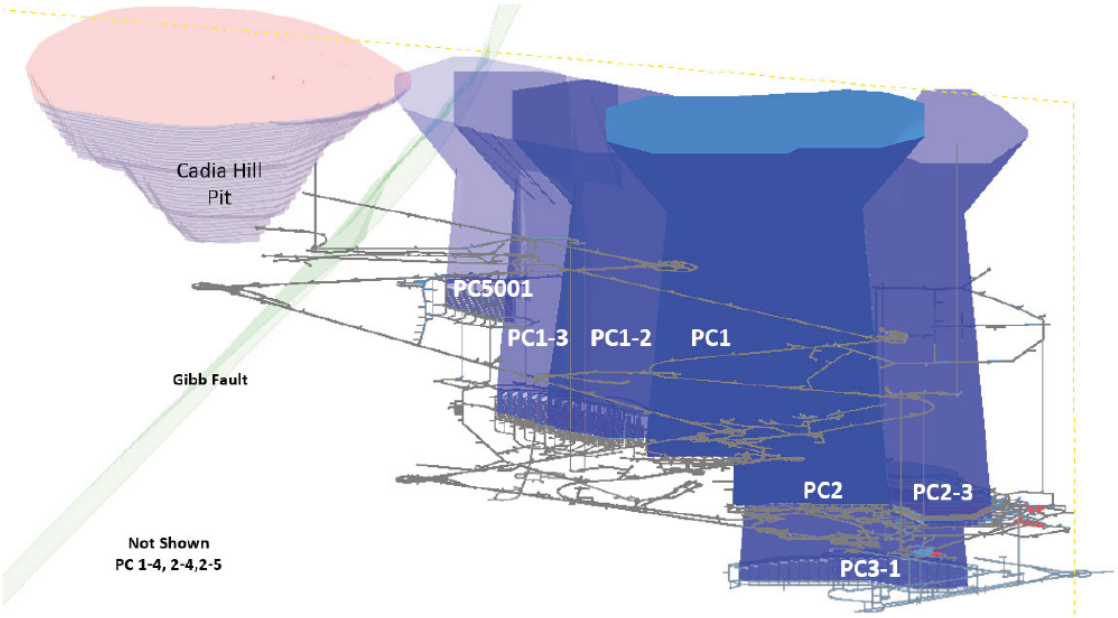

Figure 1 Location of planned Cadia East Caves in schematic section view (Newcrest Mining Limited 2021)[1]

2 Scale effect on strength

There is strong empirical evidence that the strength of rock fragments/particles decreases with increasing size due to the increased inherent heterogeneity (Bieniawski & Van Heerden 1975; Lee 1992; Hoek & Brown 1980; Yoshinaka et al. 2008). This reduction is observed at a wide spectrum of scales: particle size scale in the order of millimetres to medium scales in the order of meters depending on the degree of heterogeneity of the rock volume. In fact, it has been proposed that rock strength follows a power-law decay as size increases. The power-law function takes the form of Equation 1.

$$y = nx^{-k} \tag{1}$$

Yoshinaka et al. (2008) compared the results of testing conducted in both the laboratory and in situ on a wide range of rock types, strengths, sample shapes and sample sizes. The results of their analyses show that the value of the exponent k is influenced strongly by presence of microflaws (i.e. pores, open cracks, veins). They report that k ranges from about 0.1 to 0.3 for homogeneous hard rock, and between 0.3 to 0.9 for weathered and/or extensively microflawed rock as shown in Figure 2. The exponent k is a metric of the degree of heterogeneity of the rock mass (Pierce et al. 2009).

If the rock mass is heterogenous (k >= 0.3), the scale effect would also be evident for even larger sizes than the range of equivalent lengths shown in Figure 2. The strength of rock masses that show some degree of persistent discontinuities (open joints, large persistent weak veins, etc.) would continue to decrease for tunnel/pillar scales in the case of underground mining, and interramp-slope and global-slope scales in the case of open pit mining as shown in Figure 3. Also, strength variability is expected to be high at the laboratory scale because uniaxial compressive stress (UCS) tests can fail through various failure types such as pre-existing microdefects or healed discontinuities, intact rock, or a combination of both. As scale increases, the strength variability is expected to decrease because failure would tend to exploit and concentrate on the weakest parts of the rock mass.

1 Figure 1 has been extracted from Newcrest Mining Limited's release *Cadia PC1-2 Pre-Feasibility Study Delivers Attractive Returns* dated 19 August 2021 which is available to view at www.asx.com.au under the code "NCM" and on Newcrest's SEDAR profile. The findings in the Study and the implementation of the PC1-2 Project are subject to all necessary approvals, permits, internal and regulatory requirements and further works.

Given that rock mass strength magnitude and variability are scale-dependent properties, it is ultimately important to consider the scale at which each of the components of the caving system is being evaluated.

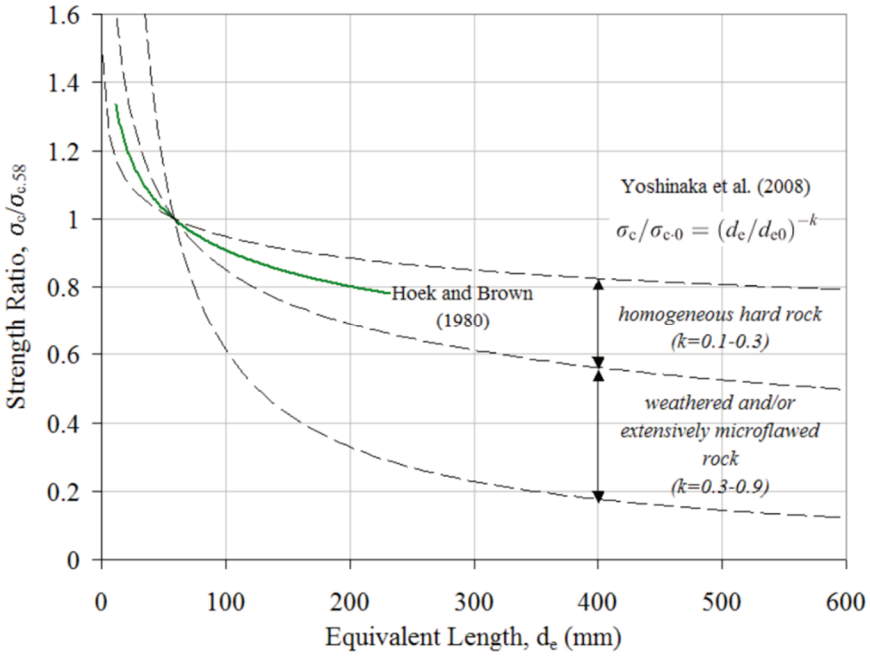

Figure 2 Scale effect relations for intact rock uniaxial compressive strength proposed by Yoshinaka et al. (2008) The relation of Hoek & Brown (1980) also is shown for comparison (from Pierce et al. 2009).

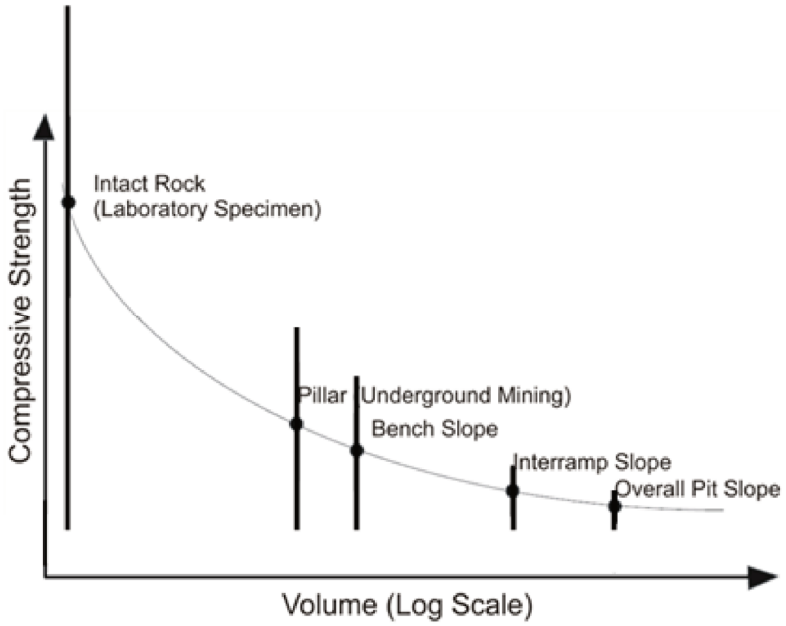

Figure 3 Conceptual schematic of the impact of scale on the median (dots) and variability (vertical lines) in rock mass strength (from Pierce et al. 2011 based on Sjöberg 1999)

3 Back-analysis of subsidence and crusher chamber stability at Cadia East mine

3.1 Large-scale caving-induced subsidence at Cadia East mine

The caving-induced subsidence was analysed using a continuum numerical model able to reproduce the emergent behaviour that is consistent with field observations. The model was built using the code *FLAC3D* (Itasca Consulting Group Inc. 2019) making use of the strain softening Itasca Model for Advanced Strain Softening constitutive model in FLAC3D, which allows for representation of modulus softening, density adjustment, dilation, dilation shutoff, scaling of properties to zone size, cohesion weakening, tension weakening, and frictional strengthening. The methodology employed to simulate the caving process was using the caving algorithm developed by Itasca (Board & Pierce 2009; Sainsbury 2012). Details of the development and constitutive model used in this analysis can be found in Ghazvinian et al. (2020).

The back-analysis was carried out from the beginning of mining at Cadia East (FY12) until April 2020 (FY20). The calibration phase of this study started in May 2020; therefore, the reconciled tonnes and field conditions up to the end of April 2020 were considered for back-analysis of FY20 and the latest mining period in the calibration process. The peak rock mass calibrated properties for the lithology (Figure 4) domains represented in the model are listed in Table 1. It is relevant to note that the rock mass properties listed in Table 1 are considered legacy properties that were inherited from previous models and were not updated based on recent logging campaigns. In the model, large-scale structures–faults were included as regions (zones) of weaker and softer material (Figure 4). The fault properties are selected based on rock mass integrity based on the fault descriptions in terms of fracturing and infill as well as core box pictures, and whether the fault core is sheared or friable (Table 2).

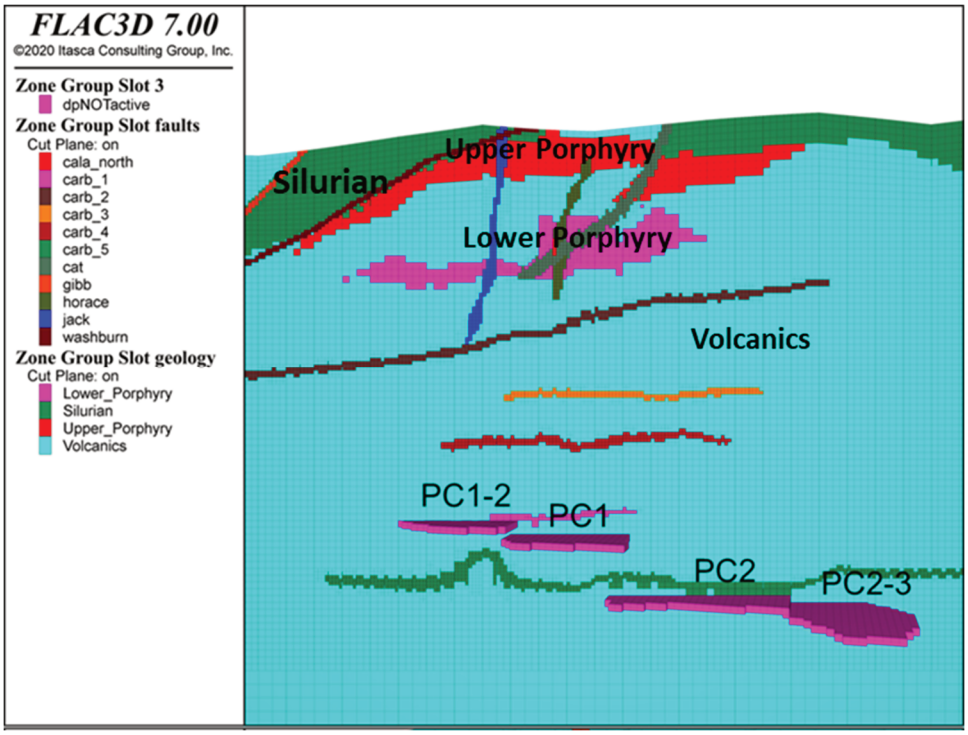

Figure 4 East–west cross-section showing the relative location of the faults and lithologies in the model

Table 1 Rock mass properties used for subsidence analysis

Lithology	Density (kg/m^3)	Geological strength index	Intact rock strength (MPa)	HB mi	Intact Young's modulus (GPa)	Dilation angle (degrees)
Volcanics	2,800	47	156	18	40	10
Silurian	2,690	30	50	12	25	10
Lower porphyry	2,780	49	168	25	45	10
Upper porphyry	2,780	43	80	20	30	10

Table 2 Fault categories based on available qualitative description and core tray pictures

Faults	Geological strength index	Uniaxial compressive strength reduction	Shearing	Keywords
Gibb	30	No	No	Clay and rock fragment/gouge
Copper gully	30	No	No	Clay and rock fragment/gouge
Cat Cat splay	30 20	Yes – 50% lower	Yes Yes	Unconsolidated shear Silurian sediment with rock fragments, gouge and clay
Cala north (FW and HW) Cala central (FW and HW) Cala west (FW and HW)	40	Yes (friable core) – 50% lower	No	Random (chaotic) fracturing with infill of calcite and the zeolitic mineral laumontite Highly friable in core
Carb1/ Carb2/ Carb3/ Carb4/ Carb5	40	No	No	Carbonate alteration, multiple quartz and carbonate-filled slip planes
Washburn	20	Yes – 50% lower	Yes	Unconsolidated shear zone of rubble 10–15 m wide
Temple	–	–	–	–
Horace	20	Yes – 50% lower	Yes	Strongly sheared Sericite-chlorite+/-clay shear
Jack	40	Yes – 50% lower	Yes	Sericitic/chloritic shears with minor puggy clay components
P2U P3U	20	Yes – 50% lower	Yes	Shear zone with multiple sericitic-chloritic+/-clay shears Clay-dominated with gouge and rock fragments

The goal of the calibration process was to match, as closely as possible, the fracture limit as was observed at the surface for FY17 through FY20 (April). The extent of the fracture limit is defined by an isosurface with a value of 0.5% for the total measure of strain (Cavieres et al. 2003). The total measure of strain is defined as:

$$\varepsilon_{tm} = \sqrt{\varepsilon_1^2 + \varepsilon_2^2 + \varepsilon_3^2}$$

where ε_1, ε_2 and ε_3 are the major, intermediate and minor principal strains, respectively.

This limit delineates the extents of visible fracturing that would be expected from orebody extraction.

The fracture limits in the field for FY17, FY18, and FY19 were established mainly based on surveyed surface fractures from drone flyovers. For FY20, the fracture limit was defined using InSAR data (75 mm/year of vertical displacement from SqueeSAR in the southern side of the crater and the metric movement (RMT) in the northern end). The Cadia East Geotechnical team completed a surface mapping campaign in April 2020. The fracture limit predicted by the model for FY20 aligns well with the observations from the mapping campaign completed as shown in Figure 5.

Those fractures are in good agreement with the fracture limit predicted by the model for FY17, FY18, FY19, and FY20 as shown in Figure 5. In general, it is observed that the calibrated model predicts the fracture limit with good proximity to field observations. Also, the large-scale structures–faults were found to have a local effect during the cave propagation and subsidence not representing a key driver in the evolution of the fracture limit over time when the cave breaks through the surface.

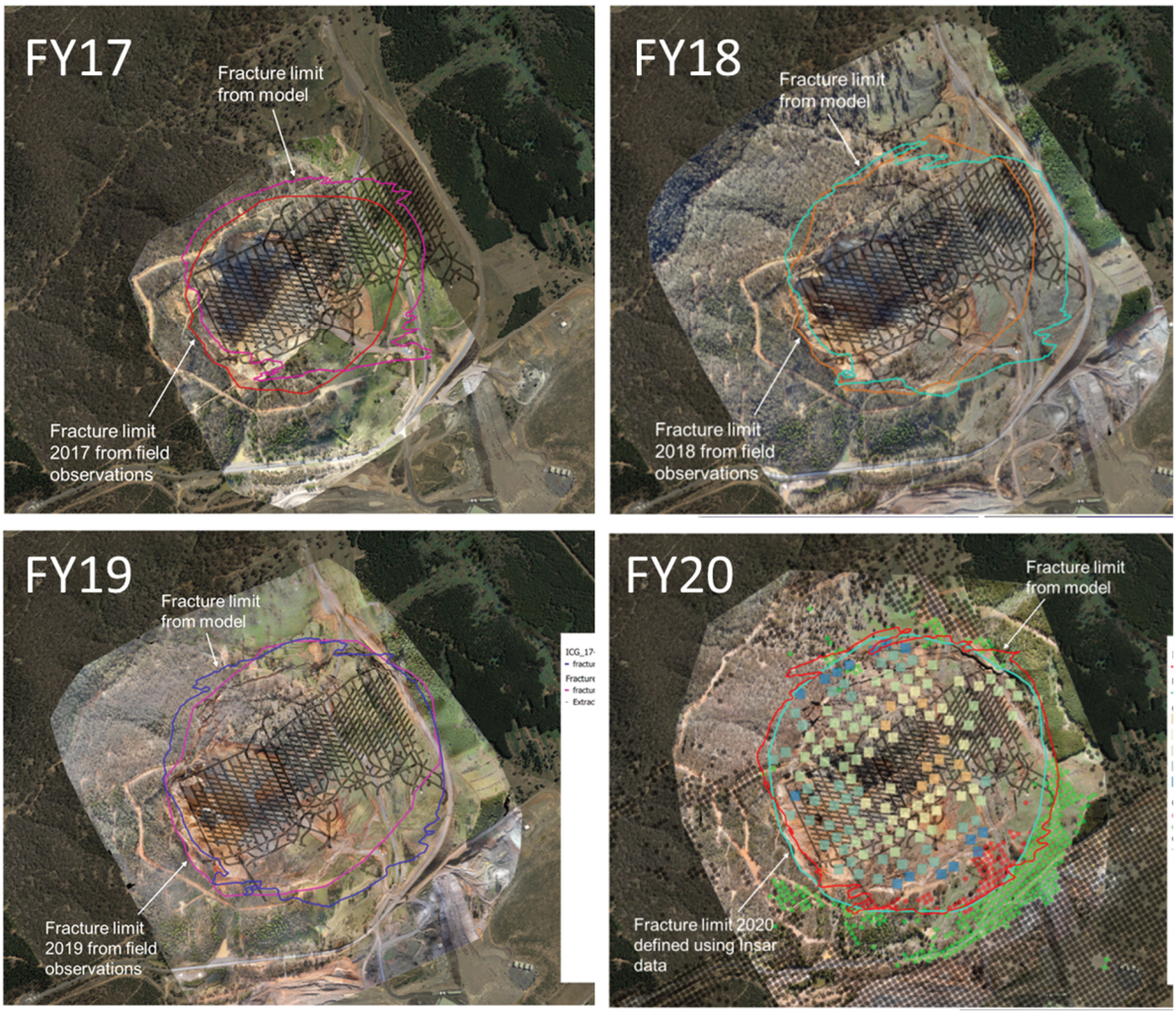

Figure 5 Comparison between the field and predicted (model) fracture limits at FY17, FY18, FY19, and FY20

The large-scale caving model is also evaluated at depth. The simulated fracture limit and mobilised zone at the end FY18 is shown in Figure 6 as a horizontal section at the 5050 engineering level (approximately mid height of cave column). The predicted fracture limit (red iso-line in Figure 6) corresponds closely to field observations of damage (cracking and slabbing of the shotcrete in the back of drives) as shown for the section of 5050-HFG-010 and 5050-HFG-007 near the intersection with 5050 MTD during FY18. The parameter plotted in Figure 6 corresponds to the percentage of peak strength loss to residual strength (termed 'sloss') which will be explained further in Section 3.2. A 'sloss' equal to approximately 0.0 matches the red isoline represented as the fracture limit. The fracture limits extents within a range of 65 m to 220 m depending on the measurement axis relative to the mobilised zone.

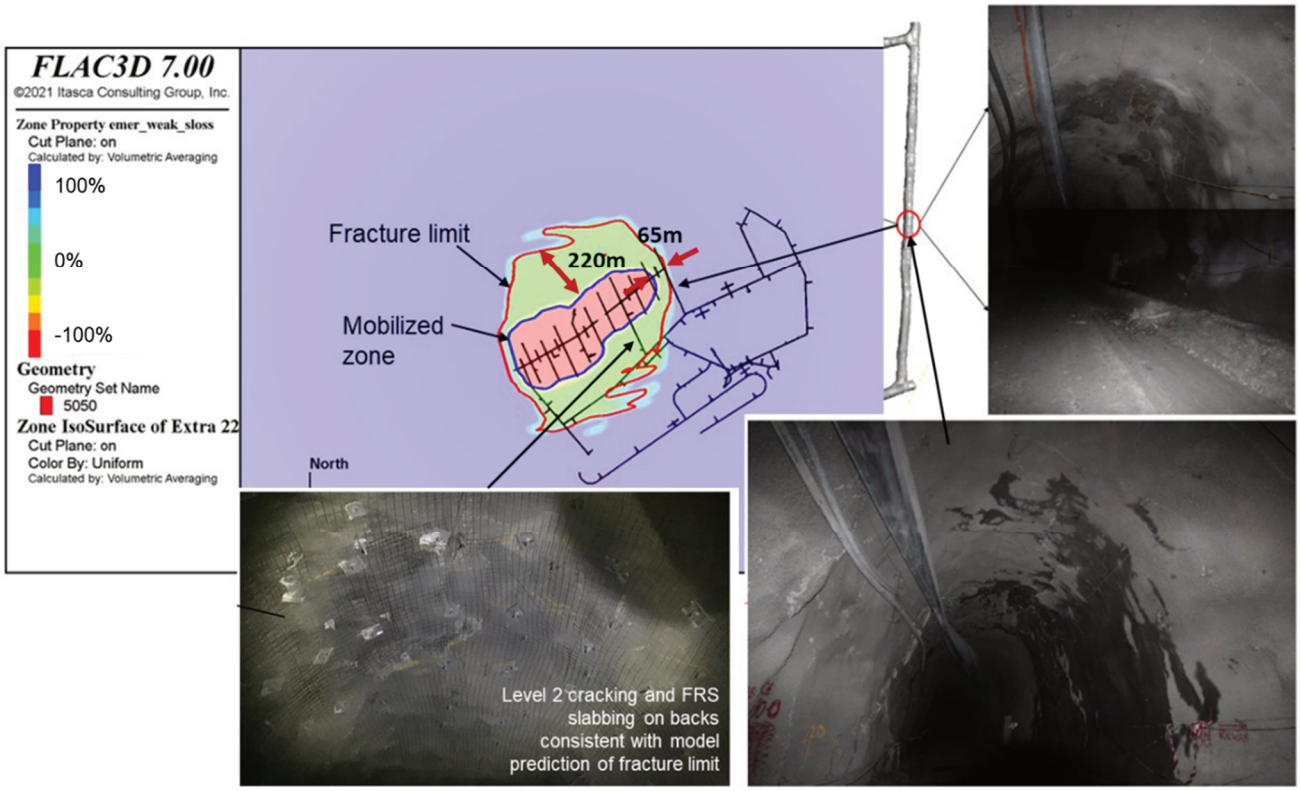

Figure 6 Fracture limit and mobilised zone at 5050 Level (FY18) from the numerical model compared to actual observations

3.2 Stability performance of crusher chamber at PC2-1

A stability assessment of the crusher chamber at PC2-1 was carried out by incorporating it into the caving model. This entailed replacing the 20 m zones in the vicinity of the excavations with refined densifications (0.5 m zones) and submitting the model to caving for simulation of production to capture the effect of cave growth and abutment loading on the crushers. Overall, the crusher chamber analysis included a back-analysis of historic observations for the PC2-1 crusher chamber to calibrate the rock mass strength at this scale.

The existing experience for the performance of crusher chambers that could be used for back-analysis and calibration of rock mass strength includes crushers for panels PC1-1, PC2-1 (2 West), and PC2-2 (2 East). Considering the available information in terms of depth of damage (probe drilling) and extensometer data (installed in the walls and backs) for PC2-1 as well as the fact that the PC2 crushers were not affected as much as the PC1 crusher by the 2017 large seismic event, the PC2-1 crusher was chosen for calibration of rock mass strength.

All of the existing and future crushers (PC1-2) are planned to be located in volcanics. The rock mass properties for volcanics listed in Table 1 were used as the starting point in the crusher analysis. However, those properties were calibrated at a cave scale which resulted in an unrealistic extension of damage at

excavation-scale. To account for rock mass behaviour at this scale, geological strength index (GSI) in the vicinity of the crusher chamber had to be increased from 47 to 60 in volcanics. This corresponds to a decrease in rock mass blockiness and improving surface quality.

The percentage of peak strength loss to residual strength (termed 'sloss') equal to approximately 0.0 is used in the simulations as a proxy for initiation of damage in the walls and back of the crushers. This threshold marks the complete loss of cohesion and the onset of bulking for the rock mass. It has been observed to manifest as fractured ground in in situ boreholes.

The depth of damage in the back of the PC2-1 crusher chamber was estimated from a few probe holes drilled during FY18 in the roof of the excavation. The probe hole data showed that the extent of damage was between 0.2–1.8 m in the back of the crusher. The observed damage in the model with a GSI of 60 was found to be in good agreement with the interpreted depth of damage from probe drilling as shown in Figure 7.

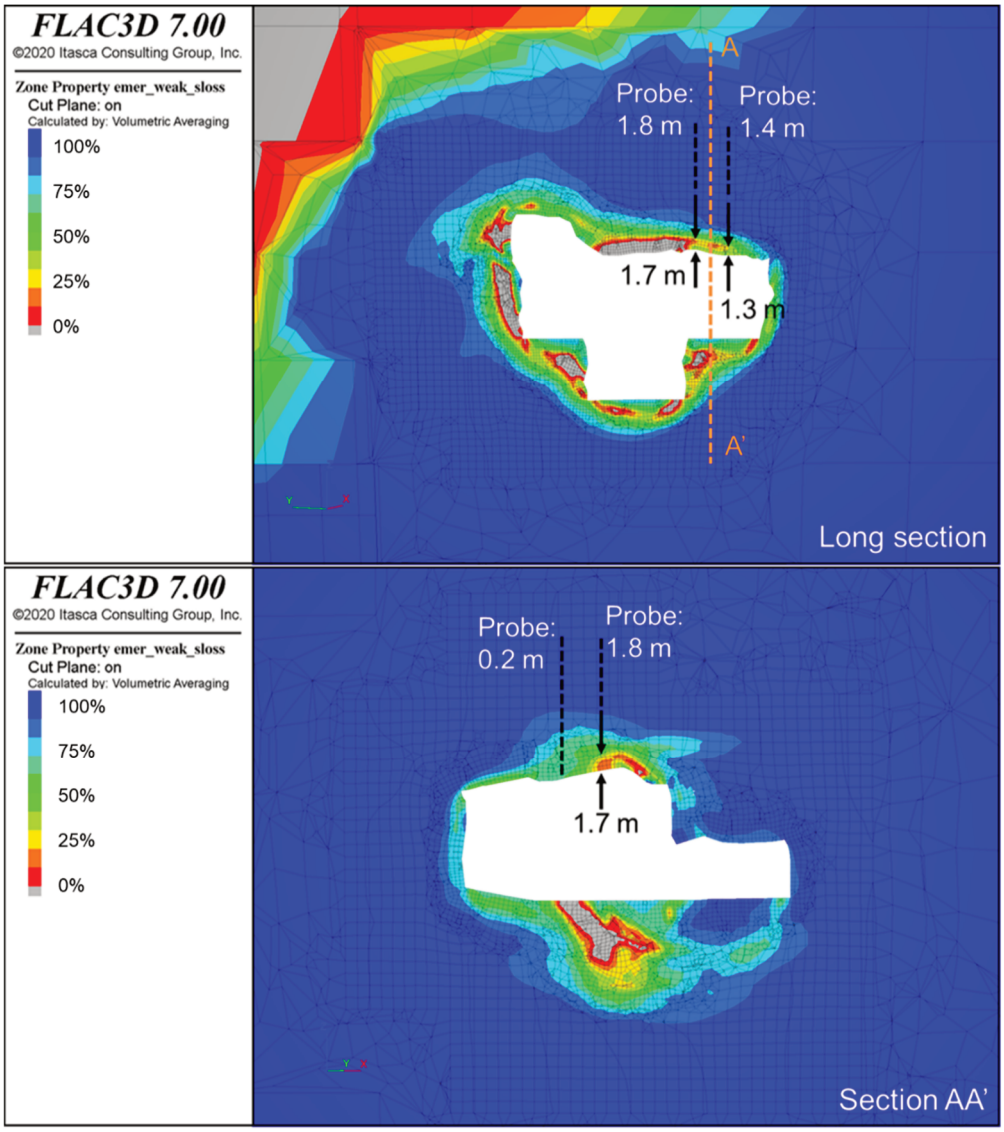

Figure 7 Comparison of simulated versus interpreted depth of damage in the back of the PC2-1 crusher chamber at FY18. Top: long section; bottom: cross-section AA'

4 Power-law fit to derive rock mass strength scale effect

As discussed in Section 2, rock strength tends to decay as size increases, following a power-law function. A logarithmic interpolation was undertaken to obtain the power-law fit to the rock mass strength at both the crusher chamber and cave scales. The resulting rock mass uniaxial compressive strengths from the

back-analysis described in Section 3 of the crusher chamber stability and caving-induced subsidence were 24.8 MPa and 7.8 MPa respectively. The scale at which these strengths need to be analysed should be dictated by the depth of yield observed at the crusher chamber and cave, which are 2–4 m and 65–220 m respectively as summarised in Table 3. Equation 2 is used to derive the k exponent and the n constant is calculated using Equation 3. The power-law fit is shown in Figure 8. The resulting constants of power-law fit are n between 31.2–36.9 and a 'k' exponent between 0.29–0.33. Based on Yoshinaka et al. (2008), a 'k' exponent of 0.3 suggests a rock mass at the limit between being homogeneous to heavily micro defected which aligns well with the volcanic rock mass characteristics observed and described at Cadia.

Table 3 Rock mass uniaxial compressive strength and scale for the crusher chamber and the caving-induced subsidence

Type of excavation	Uniaxial compressive strength rock mass (MPa)	Scale – depth of yield (m)
Crusher chamber	24.8	2–4
Cave	7.9	65-220

$$k' = -\frac{\log UCS_{cc} - \log UCS_{cs}}{\log scale_{cc} - \log scale_{cs}} \quad (2)$$

$$n' = 10^{(\log UCS_{cc} - k' * \log scale_{cc})} \quad (3)$$

where:

UCS_{cc} = uniaxial compressive strength at the crusher chamber scale.

UCS_{cs} = uniaxial compressive strength at the cave-induced subsidence scale.

$scale_{cc}$ = depth of yield at the crusher chamber.

$scale_{cs}$ = depth of yield at the cave subsidence.

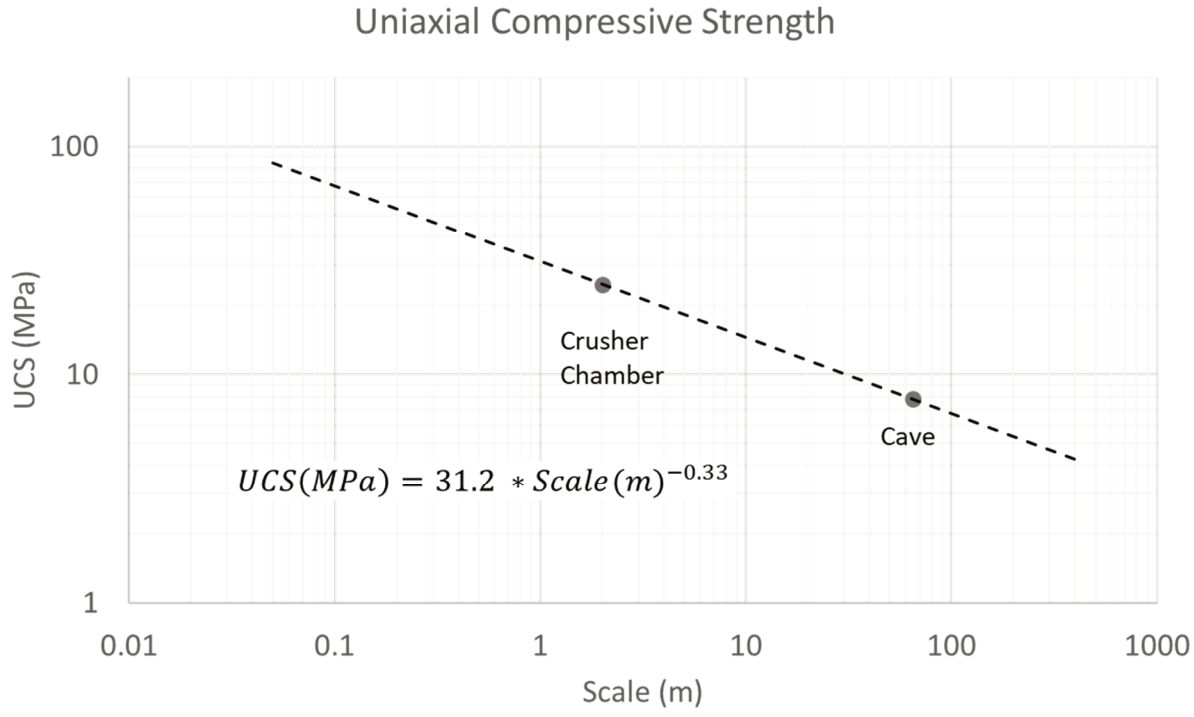

Figure 8 Power-law fit to uniaxial compressive strength at scales of crusher chamber and cave-induced subsidence

5 Discussion on a scale-dependent rock mass strength

The power-law function described in Section 4 was fitted using two data points at medium and large scales. If we consider the fitted relationship at a lab scale (0.05 m), the resulting UCS would be between 84.5–87.2 MPa which is lower than the Sigci value (156 MPa) used as part of the Hoek–Brown equation in Section 3. This may be a result of a common bias present when targeting lab tests on the stronger part of the rock mass.

A recent systematic point load test campaign was carried out at Cadia East suggesting that the Is_{50} median for the volcanics domain (considering all failure types: structural, intact and combined) is approximately 3.5 MPa. On average, the uniaxial compressive strength is 20–25 times point load strength (ISRM 2007) resulting into a median UCS lab scale between 70–87.5 MPa agreeing well with power-law fit relationship. This exercise suggests that in fact, the actual median UCS lab scale at Cadia might be lower than initially estimated which in turn results in GSI values much higher than previously assumed in order to obtain a similar rock mass strength. This makes sense given the fact that the rock mass at Cadia East is only sparsely jointed forming blocks composed of strong intact rock containing stockwork and sheeted veins (Holliday et al. 2002) which are typical characteristics of porphyry gold-copper deposits.

By rearranging the Hoek and Brown equation (assuming a Sig3 = 0, D = 0 and a = 0.5), a GSI equivalent value can be obtained by using Equation 4. Table 4 summarises GSI equivalent values obtained at both scales considered indicating that GSI should be much higher than initially proposed and also shows a decrease in GSI as scale increases, suggesting that GSI is scale-dependent property of rock masses.

$$GSI_{eq} = 9 \ln\left(\left(\frac{UCS_{scaled}}{UCS_{lab}}\right)^2\right) + 100 \quad (4)$$

Table 4 Geological strength index equivalent values obtained at the crusher chamber and cave subsidence scales.

Scale	Uniaxial compressive strength (MPa)	Geological strength index eq
Lab	73.8–80.2	–
Crusher chamber	23.8	79-80.5
Cave	7.9	58.5-60

It is also relevant to mention that depth of yield and stress-induced damage is not only a function of the peak strength but also a function of the post-peak behaviour (i.e. brittleness). In general, a higher-quality rock mass (higher GSI) with greater solid rock volume participating in the failure process often will act in a more brittle fashion. Conversely, a lower-quality rock mass (lower GSI) with higher fracture frequency often will act in a more ductile fashion. Therefore, at smaller scales (e.g. tunnel) the rock mass volume exercised at these excavations would behave in a more brittle fashion than the rock mass volume exercised at a larger scale (e.g. cave).

6 Conclusions

The importance of understanding the role of scale in rock mass strength at caving mines is discussed in this paper by describing a back-analysis of the caving-induced subsidence and the analysis of the stability performance of a crusher chamber at Cadia East mine. Based on the strong empirical evidence that rock strength decays as scale increases, a power-law function is fitted to the derived rock mass strength at the scales of the crusher chamber and cave subsidence found from the back-analysis. The fitted power-law function is then verified based on an improved rock mass knowledge derived from a recent systematic point load test campaign. This approach can be applied to study both footprint and underground infrastructure stability as well as large-scale cave propagation and cave-induced subsidence at future panels at Cadia.

Acknowledgement

The authors thank Newcrest Mining Limited for allowing the publication of this paper.

References

Bieniawski, ZT & Van Heerden, WL 1975, 'The significance of in situ tests on large rock specimens', *International Journal of Rock Mechanics and Mining Sciences & Geomechanics Abstracts*, vol. 12, issue 4, pp. 101–113.

Board, M & Pierce, M 2009, 'A review of recent experience in modelling of caving', *International Workshop on Numerical Modelling for Underground Mine Excavation Design*, June 28 2009, Asheville, in conjunction with the 43rd US Rock Mechanics Symposium.

Cavieres, P, Gaete, S, Lorig, L & Gómez, P 2003, 'Three-Dimensional analysis of fracturing limits induced by large scale underground mining at El Teniente Mine', in PJ Culligan, HH Einstein & AJ Whittle (eds), *Proceedings of the 39th U.S. Rock Mechanics Symposium*, Verlag Glückauf, Essen, pp. 893–900.

Ghazvinian, E, Fuenzalida, M, Orrego, C & Pierce, M 2020, 'Back analysis of cave propagation and subsidence at Cadia East mine', in R Castro, F Báez & K Suzuki (eds), *MassMin 2020: Proceedings of the Eighth International Conference & Exhibition on Mass Mining*, University of Chile, Santiago, pp. 535–550, https://doi.org/10.36487/ACG_repo/2063_36

Hoek, E & Brown, ET 1980, *Underground Excavations in Rock*, Institution of Mining and Metallurgy, London

Holliday, JR, Wilson, AJ, Blevin, PL, Tedder, IJ, Dunham, PD & Pfitzner, M 2002, orphyry gold–copper mineralisation in the Cadia district, eastern Lachlan Fold Belt, New South Wales, and its relationship to shoshonitic magmatism', *Mineralium Deposita*, vol. 37, pp. 100–116, https://doi.org/10.1007/s00126-001-0233-8

Itasca Consulting Group, Inc. 2019, *FLAC3D — Fast Lagrangian Analysis of Continua in Three Dimensions,* version 7, computer software, Itasca, Minneapolis.

ISRM 2007, *The Complete ISRM Suggested Methods for Rock Characterization, Testing and Monitoring: 1974-2006*, R Ulusay & JA Hudson (eds), International Society for Rock Mechanics, Lisbon.

Lee, MD 1992, *The Angles of Friction of Granular Fills*, PhD thesis, University of Cambridge, Cambridge.

Newcrest Mining Limited 2021, *Cadia PC1-2 Pre-feasibility Study Delivers Attractive Returns*, https://www.newcrest.com/sites/default/files/2021-08/210819_Cadia%20PC1-2%20Pre-Feasibility%20Study%20delivers%20attractive%20returns%20-%20Market%20Release.pdf

Pierce, M, Gaida, M & Degagne, D 2009, 'Estimation of rock block strength, in M Diederichs & G Grasselii (eds), *RockEng09: Proceedings of the 3rd Canada-US Rock Mechanics Symposium & 20th Canadian Rock Mechanics Sympsium*, Canadian Rock Mechanics Association, Toronto.

Pierce, M, O'Connor, C, Sainsbury, D, Lavoie, T, Garcia, X & Board, M 2011, *Predictions of caving and infrastructure stability in support of the feasibility study for panel caving at Oyu Tolgoi, Hugo North, Lift 1*, Itasca internal report ICG11-2619-P03-51.

Sainsbury, BL 2012, *A Model for Cave Propagation and Subsidence Assessment in Jointed Rock Masses*, PhD thesis, The University of New South Wales, Sydney.

Sjöberg, J 1999, A*nalysis of Large Scale Rock Slopes*, PhD thesis, Luleå University of Technology, Luleå.

Yoshinaka, R, Osada, M, Park, H, Sasaki, T & Sasaki, K 2008, 'Practical determination of mechanical design parameters of intact rock considering scale effect', *Engineering Geology*, vol. 96, pp. 173–186.